
# Searching for Imperfection Insensitive Externally Pressurized Near-Spherical Thin Shells

Xin Ning, Sergio Pellegrino

PII: S0022-5096(17)30805-0
DOI: 10.1016/j.jmps.2018.06.008
Reference: MPS 3365

To appear in: *Journal of the Mechanics and Physics of Solids*

Received date: 10 September 2017
Revised date: 24 May 2018
Accepted date: 6 June 2018

Please cite this article as: Xin Ning, Sergio Pellegrino, Searching for Imperfection Insensitive Externally Pressurized Near-Spherical Thin Shells, *Journal of the Mechanics and Physics of Solids* (2018), doi: 10.1016/j.jmps.2018.06.008

# Searching for Imperfection Insensitive Externally Pressurized Near-Spherical Thin Shells

Xin Ning*, Sergio Pellegrino**

*Graduate Aerospace Laboratories, California Institute of Technology, 1200 E. California Blvd., Pasadena CA 91125, USA*

**Abstract**

This paper studies the buckling behavior and imperfection sensitivity of geodesic and stellated shells subject to external pressure. It is shown that these structures can completely eliminate the severe imperfection sensitivity of spherical shells and can achieve buckling pressure and mass efficiency higher than the perfect sphere. Key results of this paper are as follows. First, a shell with the shape of an icosahedron can carry external pressure significantly higher than a spherical shell, when the effects of geometric imperfections are considered. Second, stellated shells are generally insensitive to imperfections. For pyramids with height-to-radius ratios greater than 35% the buckling pressure is greater than for a perfect sphere. The specific ratio 45% gives the highest buckling pressure, 28% higher than the perfect sphere. Third, stellated icosahedra with concave pyramids have higher mass efficiency than the perfect sphere. Fourth, in terms of volume efficiency, geodesic shells are comparable to spherical shells with a knockdown factor of 0.2 and convex stellated shells are comparable to spherical shells with a knockdown factor of 0.65.

*Keywords:* Spherical Shells, Buckling, Imperfection Sensitivity

*Current address: Department of Materials Science and Engineering, Frederick Seitz Materials Research Laboratory, University of Illinois at Urbana-Champaign, Urbana, IL 61801, USA

**Corresponding author.

*Email addresses:* ningxin87@gmail.com (Xin Ning), sergiop@caltech.edu (Sergio Pellegrino)

## 1. Introduction

The sphere is the smallest area surface that encloses a given volume, and this characteristic has made spherical shells important structural components for load-carrying and space-confinement, and also common forms in nature. The hypothetical concept of flying ships hanging from ultralight spheres with internal vacuum, proposed in the 1600's (Lana-Terzi, 1670) is still waiting for advances in structures and materials to become feasible. Recent studies by Palazotto and co-workers (Metlen, 2012; Adorno-Rodriguez and Palazotto, 2015; Snyder and Palazotto, 2017) of vacuum near-spherical structures have shown that a self-buoyant icosahedron consisting of a lightweight skin supported by a frame is now theoretically possible.

Current applications of large-scale spherical shells include gas containers in the petroleum industry, fuel tanks for rockets, deep-sea vehicles, and many others. At the micro/nano-meter scale, spherical shells have been recently used as colloidal capsules for drug delivery in biomedical engineering (Jose et al., 2014). Spherical and near-spherical shells in biological structures, such as viral capsids, have recently attracted significant attention from both academic and medical communities (May and Brooks, 2012; Mannige and Brooks, 2009; Ru, 2009; Lidmar et al., 2003).

Spherical shells subject to external pressure exhibit highly nonlinear post-buckling behavior with dramatic sensitivity to even very small imperfections (Hutchinson, 1967, 2016). In the 1930's this extreme imperfection sensitivity was identified, and Von Kármán and Tsien were among the first to carry quantitative studies of the discrepancies between theory and experiments (von Kármán and Tsien, 1939). In the 1940's, Koiter proposed a general theory of elastic stability to calculate the buckling sensitivity to small imperfections (Koiter, 1945). Following Koiter's seminal work, theoretical and experimental investigations of the imperfection sensitivity of pressurized spherical shells reached a climax in the 1960's, although it should be noted that, compared to axially loaded cylindrical shells —which also show high imperfection sensitivity— the spherical

shell research community remained smaller (Thompson, 1960; Hoff and Soong, 1963; Carlson et al., 1967). An extensive review of the literature on buckling of spherical shells has been provided by Hutchinson (2016).

Currently, there is renewed interest in this topic, motivated by recent advances in digitally-based design and shape optimization, as well as fabrication technologies that have enabled precisely engineered shapes (Lee et al., 2016,b; Jimenez et al., 2017). In parallel, advances in the life sciences have drawn attention to medical implications of the buckling of spherical (or sphere-like) viral and colloidal capsules under external osmotic pressure (Kim et al., 2014; Datta et al., 2014; Vliegenthart and Gompper, 2011). Recent research has focused on differences in behavior caused by changing the boundary conditions from dead pressure to volume control (Thompson and Hutchinson, 2017).

From a practical perspective, current methods for the design of spherical shells under external pressure are still primitive. The empirical knockdown-factor method is the main method to account for the reduction in theoretically estimated buckling pressure due to imperfections. The buckling pressure is estimated from:

$$P_{cr} = \gamma P_{cl} \tag{1}$$

where $\gamma$ is an empirically based knockdown factor and $P_{cl}$ is the classical buckling pressure of a perfect shell (Zoelly, 1915):

$$P_{cl} = \frac{2E}{\sqrt{3(1-\nu^2)}}\left(\frac{t}{R}\right)^2 \tag{2}$$

where $E$, $\nu$, $t$, and $R$ are respectively the Young's modulus, Poisson's ratio, thickness and radius of the shell.

Krenzke and Kiernan (1963) proposed $\gamma = 0.7$ as an empirical lower-bound knockdown factor for designing spherical shells. However, it was later argued that early experimental results were too scattered, mainly due to the lack of precise control of imperfections during fabrication (Kaplan and Fung, 1954; Homewood et. al., 1961; Seaman, 1962).

There are three main issues with the knockdown factor method. First, since

this method was proposed several decades ago, it does not represent current materials, design methods, and manufacturing technologies (Nemeth and Starnes, 1998). Second, currently used knockdown factors are not accurate as they were not based on systematic, extensive experimental studies (Nemeth and Starnes, 1998). In fact, recent results have shown that $\gamma = 0.2$ would be a better choice (Lee et al., 2016,b; Jimenez et al., 2017). Third, it leads to inefficient structural designs because nearly 80% of the structure's theoretical loading capability is lost due to the reduction by $\gamma$.

An alternative approach, which has already been successful for cylindrical shells, would be to add closely spaced stiffeners in both circumferential and meridional directions of a spherical shell. However, it has been found that the buckling pressure of stiffened spherical shells is actually smaller than for unstiffened shells with the same weight (Krenzke and Kiernan, 1963). Other configurations of the stiffeners may perform better, but the number of studies of externally pressurized, stiffened spherical shells is currently quite limited (Singer et al., 2002; Ventsel and Krauthammer, 2001).

The approach proposed in this paper is fundamentally different, and was inspired by the authors' recent research on imperfection-insensitive axially loaded cylindrical shells (Ning and Pellegrino, 2013, 2015; Ning, 2015; Ning and Pellegrino, 2017). For cylindrical shells it has been shown that extreme imperfection sensitivity can be greatly decreased or even eliminated by choosing structural shapes that break the exact axial symmetry of the cylinder. Specifically, this was done by introducing a wavy cross-section. Extending the idea of avoiding total symmetry in the design of thin shells, to enhance imperfection-sensitive behavior, this paper explores the buckling behavior and imperfection sensitivity of a range of externally pressurized sphere-like thin shells with polyhedral shapes.

This paper is organized as follows. Section 2 defines the shell geometries that are considered. The buckling behavior and imperfection sensitivity of geodesic shells are then presented in Section 3. Section 4 presents parametric studies of the behavior of stellated shells. Sections 5 and 6 discuss the mass and volume

efficiencies of these shells, and Section 7 concludes the paper.

## 2. Geometry of Near-Spherical Shells

The shell geometry is based on the icosahedron, chosen because it is the regular polyhedron formed of triangles that provides the closest approximation to the sphere. It encloses a larger volume than other regular polyhedra with the same circumscribed sphere. The subdivision of the icosahedron into smaller triangles leads to geodesic shells, whose geometry has already been studied extensively (Fuller, 1965; Tarnai, 1996). In addition, it has been found that inverting every pyramid of a geodesic dome into a concave shape, a transformation known as "dimpling", can significantly increase its stiffness (Kitrick, 1983; Tarnai, 1989). The choice of this particular basic shape for the present study provides access to a large design domain, controlled by only a small number of design variables.

Two families of shells are considered, *geodesic shells* and *stellated shells*. The first family provides close approximations to the sphere. The second family is based on the first, but each triangular face is replaced by a pyramid, in order to achieve a more stable design.

### *2.1. Geodesic Shells*

The icosahedron has 20 identical equilateral triangular faces, 30 edges, and 12 vertices, as shown in Fig. 1. A geodesic shell is obtained by subdividing the faces of an icosahedron into smaller, identical equilateral triangles, and then projecting the additional vertices onto the circumscribed sphere. The initial subdivision is shown in Fig. 2. The solid dots are the original vertices of the icosahedron, and the hollow dots are the intermediate vertices obtained by subdividing the faces of the icosahedron. The second-order subdivision splits each edge into two equal segments and creates four equilateral triangles, see Fig. 2b. Similarly, the $n^{th}$-order subdivision divides each edge of each face of the icosahedron into $n$ equal segments and creates $n^2$ equilateral triangles.

The additional vertices of the subdivision are then radially projected onto the circumscribed sphere, as shown in Fig. 3 (for clarity, only one face has been

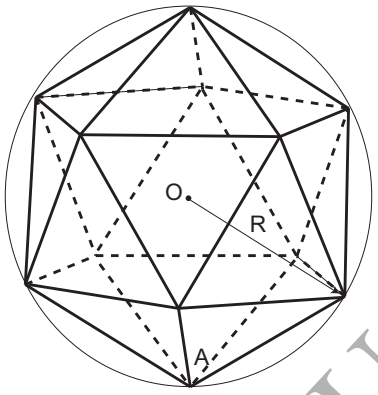


Figure 1: Icosahedron and its circumscribed sphere. $R$ and $O$ denote the radius and center of the circumscribed sphere. Point $A$ is the lowest vertex.

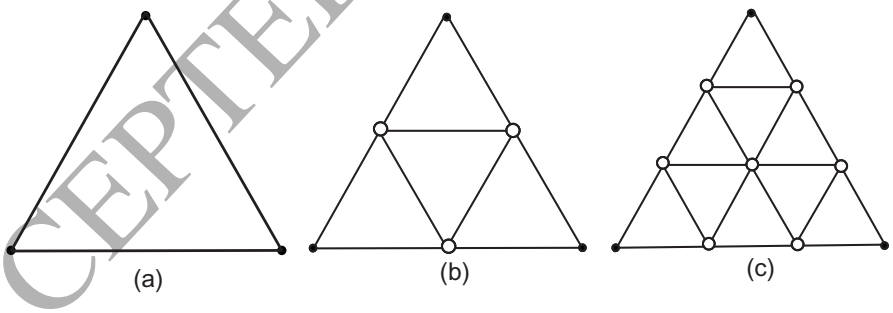


Figure 2: Schematic of subdividing a face of icosahedron into faces of a geodesic sphere. (a) A face of icosahedron (first-order subdivision). (b) Second-order subdivision. (c) Third-order subdivision.

shown) for the case $n = 2$, to form the faces of a geodesic shell. Note that the triangles are distorted by the projection and are no longer equilateral (Van Loon, 1994).

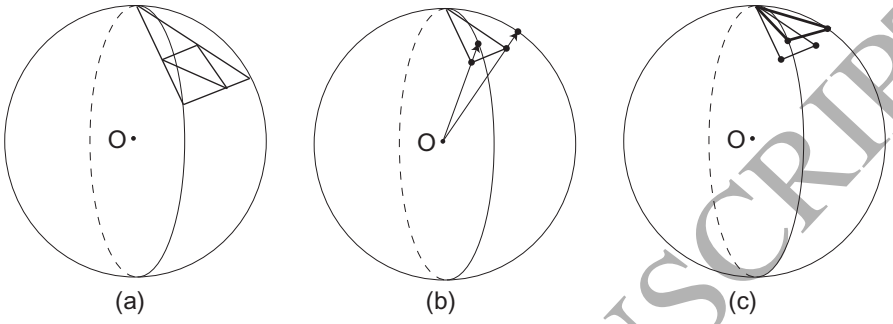


Figure 3: Schematic of creating a face of a geodesic shell. The circular arcs lie on the circumscribed sphere of the icosahedron.

Geodesic shells with second- to fifth-order of subdivision are shown in Fig. 4. The figure clearly shows that higher order of subdivision leads to geometries closer to the sphere.

The geodesic shell defined by the $n^{th}$-order subdivision of the icosahedron is denoted as *$n^{th}$-order geodesic shell*, and the undivided icosahedral shell is denoted as $1^{st}$-order geodesic shell.

### *2.2. Stellated Shells*

A stellated shell is obtained by replacing each face of a geodesic shell with a pyramid. The center point of each face (point C in Fig. 5) is radially projected outward to obtain a convex pyramid, with height $H > 0$ (Fig. 5a), or inward to obtain a concave pyramid, with height $H < 0$ (Fig. 5c). Connecting point T to the original vertices of the face defines three new identical triangular faces, forming a pyramid with apex at point T. It should be noted that the vertices of the original geodesic shells still lie on the circumscribed sphere, only the apices of the pyramids lie inside or outside the circumscribed sphere.

The stellated shell created from the $n^{th}$-order geodesic shell is denoted as *$n^{th}$-order stellated shell*. Convex stellated shells have $H > 0$; concave stellated

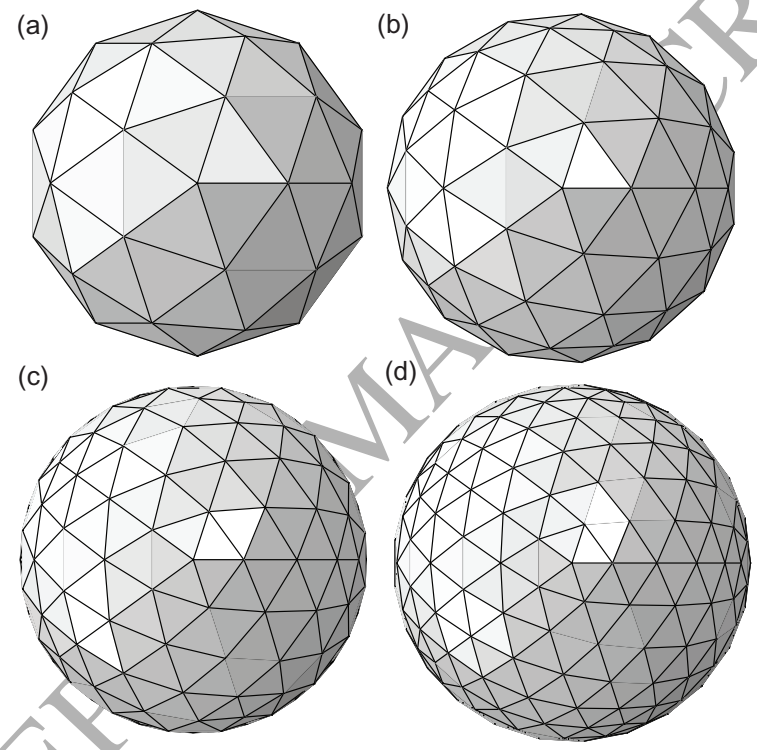


Figure 4: (a) Second-order to (d) fifth-order geodesic shells.

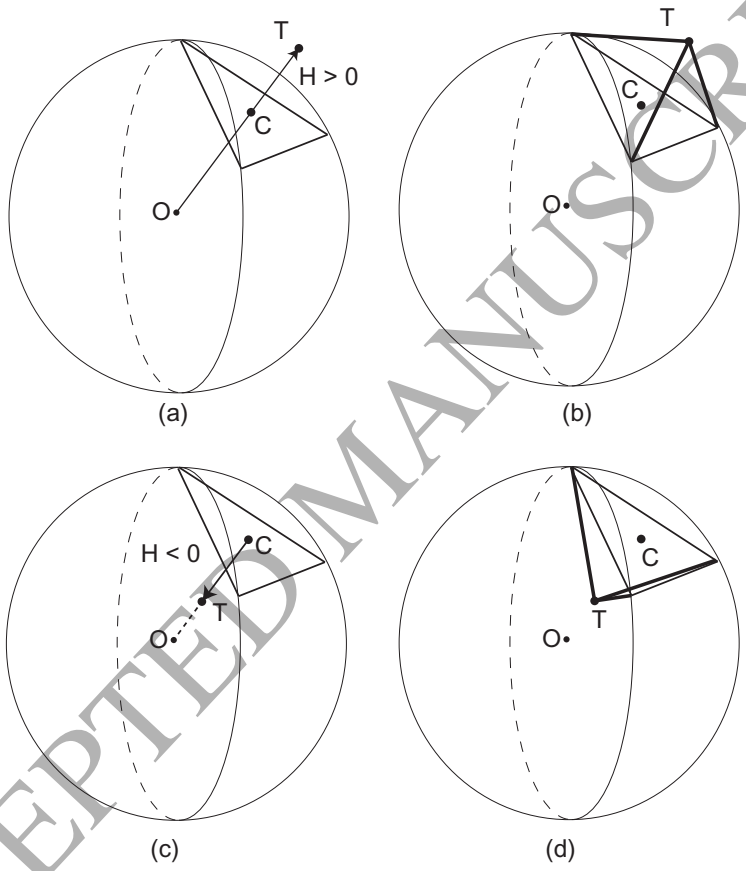


Figure 5: Schematic of creating stellated shells with convex (a-b) and concave (c-d) pyramids.

shells have $H < 0$. Fig. 6 shows $1^{st}$- and $2^{nd}$-order stellated shells.

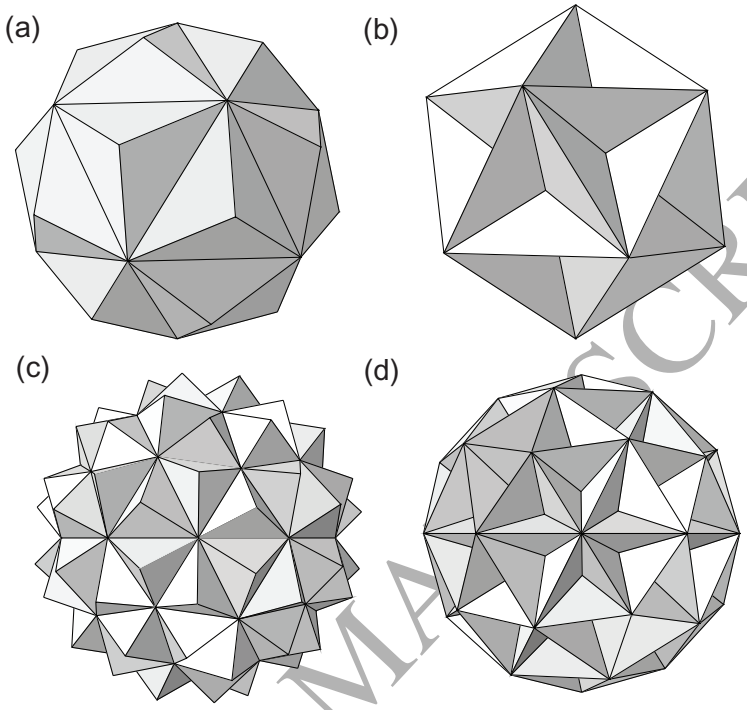


Figure 6: $1^{st}$-order stellated shells with (a) $H = 0.25R$ and (b) $H = -0.25R$. $2^{nd}$-order stellated shells with (c) $H = 0.25R$ and (d) $H = -0.25R$.

## 3. Buckling and Imperfection Sensitivity of Geodesic Shells

Geodesic shells with various radius-to-thickness ratios ($R/t$) have been numerically analyzed in order to study the sensitivity of the buckling pressure to geometrical imperfections. This section presents the finite element simulation techniques for the buckling analysis. Parametric results for the buckling pressure of both geometrically perfect and imperfect geodesic shells, and for the sensitivity to the amplitude of the geometric imperfections are also presented.

### 3.1. Finite Element Modeling

All shells considered in this paper are derived from the icosahedron in Fig. 1. This $1^{st}$-order geodesic shell serves as an example for describing the simulation methods. The diameter of the circumscribed sphere is 0.1 m, and $R/t$ varies from 100 to 200. The material is assumed linear-elastic, with Young's modulus and Poisson's ratio of 68.9 GPa and 0.3 (Aluminum), respectively. Material nonlinearity and failure are not considered.

The commercial finite element package Abaqus/Standard 6.14 was used to calculate the critical buckling mode and the corresponding buckling pressure. A linear eigenvalue buckling analysis was carried out to compute the critical buckling mode. The critical buckling pressure was computed by a load-displacement arc-length incrementation nonlinear analysis using the Riks solver. The first limit pressure in the load-displacement curve was defined as the critical buckling pressure. Fully-integrated triangular thin shell elements (element S3) were used. The size of the shell elements was determined by a mesh sensitivity study, leading to a maximum element size of 1.5 mm. All of the six degrees of freedom of the lowest vertex A, shown in Fig. 1, were held fixed in the simulation. The shell was subject to uniform external pressure, defined as a follower load perpendicular to the shell surface.

Because the actual imperfections of sphere-like shells are unknown until these shells are fabricated, the imperfection shape was chosen to be the first (critical) buckling mode, which is one of the worst imperfections for buckling and is commonly used in the literature (Hutchinson, 1967, 2016). Imperfections of various amplitudes were considered, including both positive and negative signs, to account for the three types of buckling (stable, unstable, and asymmetric buckling) that may be exhibited by different shells (Ning and Pellegrino, 2015, 2017).

The NURBS-based CAD software Rhino 3D (version 5.0) was used to create CAD models for the *perfect geometry* of the shell and to export Initial Graphics Exchange Specification (.IGS) files for finite element analyses. Abaqus/CAE was used to read the .IGS file, set up the finite element models, and to compute

the critical buckling pressures and buckling modes. Both the generation of CAD models and finite element analyses were automated by means of Python scripts. Note that the linear eigenvalue analysis for finding the buckling mode was only performed for geometrically perfect shells. Next, the displacements of the nodes according to the first buckling modes were extracted from the Abaqus/Standard output file and were scaled with the maximum displacement equal to the amplitude of the imperfection. Two models of imperfect shells (with positive and negative imperfection amplitudes) were obtained by superposing the scaled displacements on the mesh of the perfect shell. For the perfect geometry and also for each of the imperfect geometries, the critical buckling pressures of perfect and imperfect shells were then computed with the Riks solver. Details on this type of analysis can be found in Section 3.3 of (Ning and Pellegrino, 2015). The buckling pressures of the perfect shell, and of imperfect shells with positive and negative imperfection amplitudes are denoted as $P_0$, $P_+$, $P_-$, respectively.

### *3.2. Buckling of Perfect Geodesic Shells*

The buckling of first- to fifth-order geodesic shells was analyzed using the above technique. For each shell, five $R/t$ values (100, 125, 150, 175, and 200) were considered. The critical buckling pressure of geometrically perfect geodesic shells ($P_0$) are presented in Fig. 7. The buckling pressure of spheres with the same radius, obtained from Eq. 2, are included for comparison.

Fig. 7 shows, for each type of structure, a linear relation with negative slope between $P_0$ and $R/t$ in the log-log plot, corresponding to a power-law relationship. i.e. the buckling pressure rapidly decreases as the shell becomes thinner, but decreases at different rates for different shells. Therefore, the buckling pressure of geodesic shells follows the relationship:

$$P_0 = k\frac{2E}{\sqrt{3(1-\nu^2)}}\left(\frac{t}{R}\right)^{-\alpha} \tag{3}$$

where $\alpha$ is the slope and $k$ is a constant that accounts for the order of subdivision. Comparing Eq. 3 with Eq. 2, $\alpha = -2$ and $k = 1$ for spherical shells.

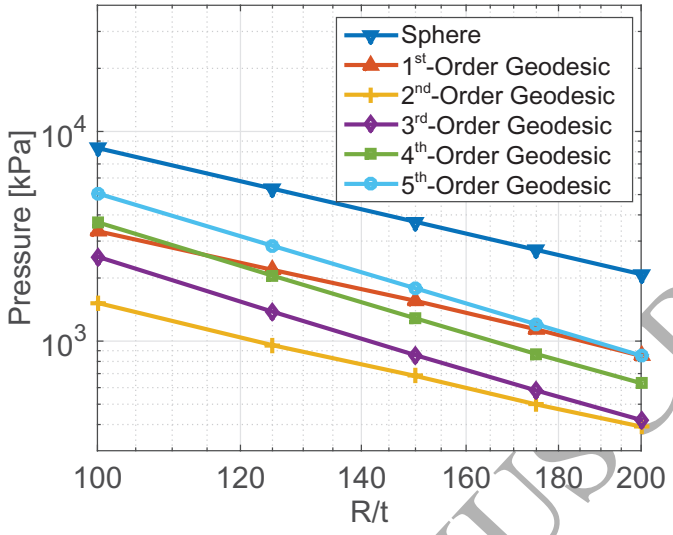


Figure 7: Critical buckling pressures of geometrically perfect spherical and geodesic shells, plotted against $R/t$ in log-log scales.

The values of $\alpha$ and $k$ are presented in Table 1. The table shows that the buckling pressures of the $1^{st}$- and $2^{nd}$-order geodesic shells decrease more slowly than the sphere, as $R/t$ increases, and that the buckling pressures of $3^{rd}$-, $4^{th}$-, and $5^{th}$-order geodesic shells decrease at similar rates and much faster than the sphere. The values of $k$ in the table were computed by a linear fitting based on the results in Fig. 7.

Table 1: Values of $\alpha$ and $k$ in Eq. 3.

| Shell | $\alpha$ | $k$ |
|---|---|---|
| Sphere | -2 | 1 |
| $1^{st}$-order geodesic | -1.9654 | 0.3460 |
| $2^{nd}$-order geodesic | -1.9592 | 0.1495 |
| $3^{rd}$-order geodesic | -2.5909 | 4.5384 |
| $4^{th}$-order geodesic | -2.5560 | 5.6704 |
| $5^{th}$-order geodesic | -2.5691 | 8.3412 |

Therefore, the buckling pressure of geodesic shells can be computed using

the values of $k$ and $\alpha$ from Table 1. For example, the buckling pressure of $3^{rd}$-order geodesic shells has the expression:

$$P_0 = 4.5384 \frac{2E}{\sqrt{3(1-\nu^2)}} \left(\frac{t}{R}\right)^{-2.5909} \tag{4}$$

It is interesting to consider how the buckling pressure changes with the order of subdivision. It is shown in Fig. 7 that the change is non-monotonic, i.e. the buckling pressure decreases significantly when the subdivision increases from the first to the second order, and then increases for higher-order subdivision. The infinite order shell (sphere) has the highest buckling pressure.

The buckling modes, obtained from linear eigenvalue analyses of five structures with $R/t = 100$ and different order of subdivision, are shown in Fig. 8. The buckling modes consist of half waves confined within a face. The symmetry of the buckling modes changes as the order of subdivision increases. Note that all shells have 5-fold rotational symmetry with respect to the top-bottom axis. However, only the buckling modes of high order geodesic shells, i.e. the $4^{th}$-order and the $5^{th}$-order, exhibit 5-fold rotational symmetry. The buckling modes of lower order geodesic shells exhibit mirror symmetry. Both types of symmetry are shown in Fig. 8.

### *3.3. Imperfection Sensitivity*

Geometric imperfections were introduced in the geodesic shells to study their influence on the buckling pressure. The imperfections have the shape of the critical buckling mode and amplitude of one shell thickness. Both positive and negative amplitudes of imperfection were analyzed, and their buckling pressures are denoted as $P_+$ and $P_-$, respectively. The knockdown factor $\gamma$, used to quantify the influence of imperfections, is defined as:

$$\gamma = \frac{\min(P_+, P_-)}{P_0} \tag{5}$$

where $P_0$ is the buckling pressure of a perfect shell. Note that the lower of $P_+$ and $P_-$ is considered as the critical buckling pressure of the imperfect shell.

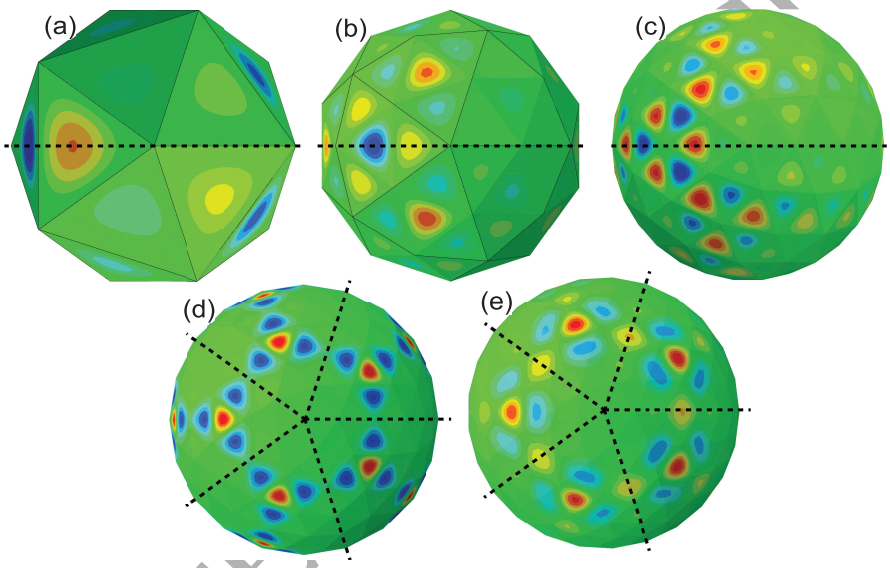


Figure 8: Buckling modes of $1^{st}$- to $5^{th}$-order geodesic shells (a-e) with the dash lines showing mirror or rotational symmetries. Note that the color contours represent the radial displacements, where red and blue colors correspond to outward and inward deformation. $R/t$ is 100 for all plots.

The knockdown factors for all of the shells considered in the previous section have been plotted in Fig. 9. The figure shows that the first-order geodesic shell (icosahedron) has the highest knockdown factors (0.9757 to 1), indicating that it is insensitive to imperfections of one shell thickness. $2^{nd}$-order geodesic shells have slightly lower knockdown factors than the icosahedron but they are still close to one (0.9669 to 0.9990) for all $R/t$ ratios. The figure also shows that higher order of subdivision leads to lower knockdown factors, with geodesic shells approaching the sphere as the order of subdivision increases and the knockdown factor decreases. It should be noted that the knockdown factor of spherical shells is 0.2 for $R/t$ ranging from 100 to 300 with imperfection amplitudes larger than one shell thickness (Hutchinson, 2016; Lee et al., 2016b). These analyses were not repeated in the present study.

Fig. 9 also shows that the dependence between $\gamma$ and $R/t$ is low with a small trend of increasing $\gamma$ with respect to $R/t$. For example, the knockdown factors of the $1^{st}$- and $5^{th}$-order geodesic shells increase by 0.25% and 20.3%, respectively, as $R/t$ increases by 100%.

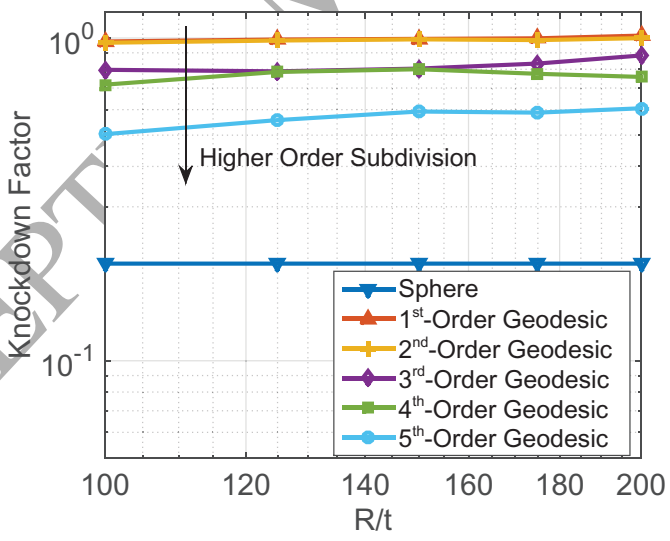


Figure 9: Knockdown factors of geodesic shells with different values of $R/t$.

The buckling pressures of imperfect shells ($\gamma P_0$) have been plotted in Fig. 10.

Although the buckling pressure of perfect spheres is significantly higher, due to the lower imperfection sensitivity of geodesic shells, the buckling pressures that account for imperfections are close to or even higher than for imperfect spherical shells. The buckling pressures of imperfect $1^{st}$-order geodesic shells are the highest among all shells considered so far. The buckling pressures of $4^{th}$- and $5^{th}$-order imperfect geodesic shells are similar and also significantly larger than the imperfect spherical shells.

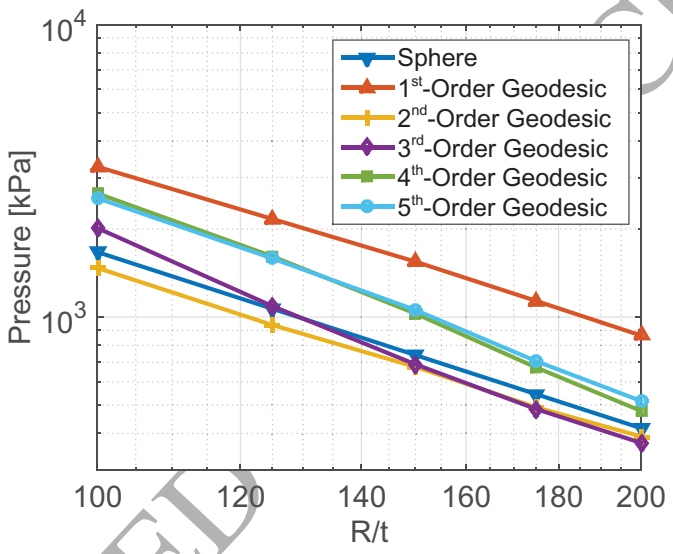


Figure 10: Buckling pressures of geometrically imperfect geodesic shells with different values of $R/t$. The imperfection amplitude is equal to one shell thickness for all results in this figure.

In summary, the results presented in this section indicate that: 1) geodesic shells can significantly reduce the imperfection sensitivity under external pressure; 2) the knockdown factors show a low dependence on radius-to-thickness ratio; 3) $1^{st}$- and $2^{nd}$-order geodesic shells are insensitive to imperfections; and 4) geodesic shells can achieve similar or significantly higher load-carrying capability than spherical shells when the effects of imperfections are considered.

### *3.4. Influence of Imperfection Amplitude*

In the previous section the imperfection amplitudes were set equal to one shell thickness. In this section, various amplitudes of imperfection ($\beta$) are considered, while keeping a fixed $R/t = 100$.

The knockdown factors of $1^{st}$- to $5^{th}$-order geodesic shells, with imperfection amplitudes up to 2 times the shell thickness are presented in Fig. 11. The shape of the imperfection is the critical buckling mode, calculated from a linear eigenvalue analysis. According to the figure, the knockdown factor of the $1^{st}$- and $2^{nd}$-order geodesic shells is reduced by less than 5%, even for the largest imperfection, further proving that these shells are not sensitive to imperfections. On the other hand, significant reductions in the knockdown factors of $3^{rd}$- to $5^{th}$-order geodesic shells are found when the imperfection amplitude increases.

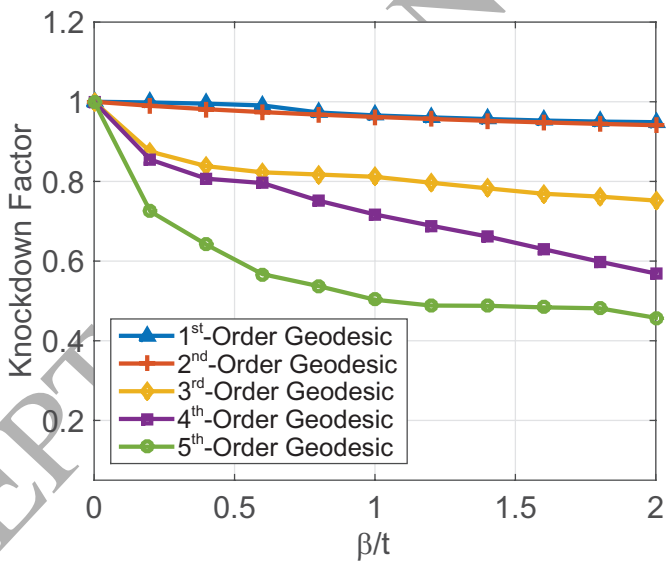


Figure 11: Knockdown factors of geodesic shells, plotted against normalized imperfection amplitude.

## 4. Buckling and Imperfection Sensitivity of Stellated Shells

This section presents a series of parametric studies of stellated shells with $R/t = 100$. The heights of the pyramids range from $H = -0.5R$ (concave pyramids) to $H = +0.5R$ (convex pyramids). The buckling pressure and imperfection sensitivity of $1^{st}$-order stellated shells are considered first, followed by a study of higher-order stellated shells.

### *4.1. $1^{st}$-Order Stellated Shells*

Fig. 12 shows a plot of the buckling pressure of geometrically perfect $1^{st}$-order stellated shells ($P_0$), normalized by the buckling pressure of a perfect spherical shell ($P_s$) and plotted against the height of the pyramids ($H$). Rather strikingly, the relationship is approximately piecewise linear: $P_0/P_s$ increases monotonically in the ranges $H \leq -0.25R$ and $0.05R \leq H \leq 0.45R$, and it decreases in the ranges $-0.2R \leq H \leq 0.05R$ and $H \geq 0.45R$. Note that the lowest point in the plot in Fig. 12 corresponds to $H \approx 0$ (in which case the $1^{st}$-order stellated shell becomes an icosahedron), which means that almost all $1^{st}$-order stellated shells have a larger buckling pressure than the $1^{st}$-order stellated shell. Indeed, $1^{st}$-order stellated shells with tall, convex pyramids ($H \approx 0.35R$) have very high buckling pressure, even higher than a geometrically perfect sphere.

The critical buckling modes of four representative $1^{st}$-order stellated shells, with $H/R = -0.5, \ -0.1, \ +0.1$ and $+0.5$, plotted in Fig. 13, show significant changes which can explain the observed changes in buckling pressure variation. The shells with deep concave pyramids exhibit localized buckling modes (Fig. 13a) where only a few faces buckle significantly, into a half-wave mode, while the other faces deflect by small amounts. Moreover, the edges of the pyramids do not deform, forming a sort of rigid frame for the shell. As the the height of the concave pyramids decreases, the buckling mode becomes more global (Fig. 13b). The three faces of each pyramid deform significantly, forming a half-wave dimple across the whole pyramid. The edges of the pyramids also

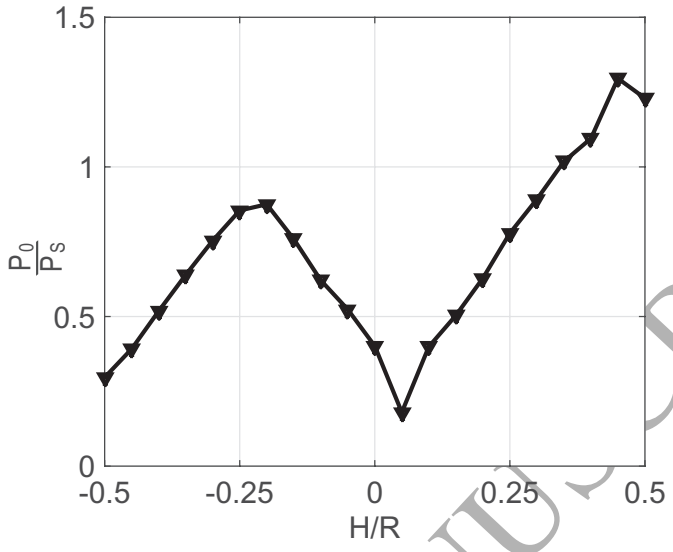


Figure 12: Variation of buckling pressure of geometrically perfect $1^{st}$-order stellated shells with pyramid height.

deform significantly. In the case of shallow convex pyramids (Fig. 13c), only two faces of each pyramid show significant deflections, whereas the third face does not deflect. Finally, in shells with highly convex pyramids (Fig. 13d) the buckling mode resembles the highly concave case.

A comparison between the buckling pressures of geometrically imperfect $1^{st}$-order stellated shells and the corresponding perfect shells, in Fig. 14, shows that almost all $1^{st}$-order stellated shells are rather insensitive to imperfections. In this figure, note that imperfect stellated shells with $H \geq 0.35R$ can carry higher external pressure than even a perfect sphere. It is particularly significant that the shell with $H = 0.45R$ has the highest buckling pressure for both perfect and imperfect geometries, respectively 29% and 28% higher than the perfect sphere. Its knockdown factor of 0.9556 indicates that this particular shell design is insensitive to imperfections.

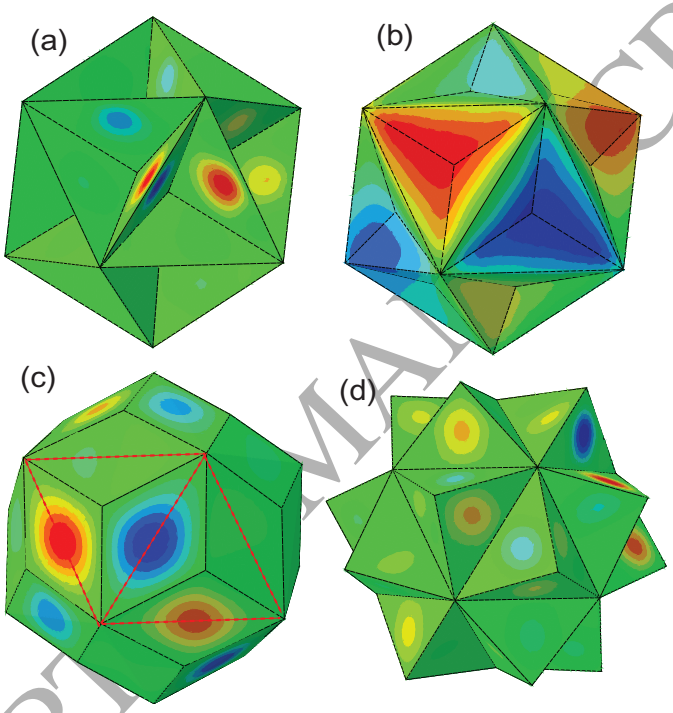


Figure 13: Buckling modes of $1^{st}$-order stellated shell with (a) $H = -0.5R$, (b) $H = -0.1R$, (c)$H = 0.1R$, and (d) $H = 0.5R$. The dash lines in (c) illustrate the base face of two adjacent pyramids.

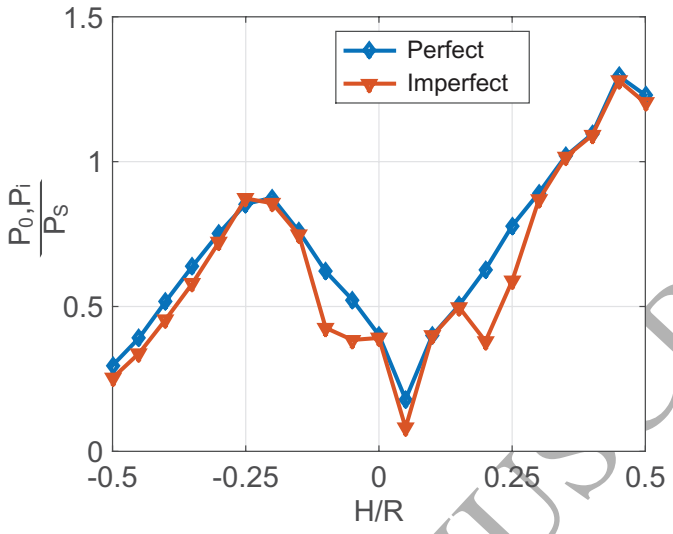


Figure 14: Variation of buckling pressure of perfect ($P_0$) and imperfect ($P_i$) $1^{st}$-order stellated shells with pyramid height ($H$). $P_0$ is normalized by the buckling pressure of the perfect sphere ($P_S$), where $P_i = min(P_+, P_-)$.

### *4.2. $2^{nd}$- to $5^{th}$-Order Stellated Shells*

The buckling pressure ($P_0$) of geometrically perfect $2^{nd}$- to $5^{th}$-order stellated shells with pyramid heights ranging from $-0.5R$ to $0.5R$ are presented in Fig. 15. In general, the buckling pressure is increased by increasing the order of the subdivision. For each specific subdivision, the variation of $P_0$ with $H$ is broadly similar to the results for stellated icosahedra, in Fig. 12, although the piecewise linear shape of the plot is less definite. For convex stellated shells, higher buckling pressure can be achieved with lower $H$ than for the $1^{st}$-order stellated shell, but for larger $H$ there is a plateau. The highest buckling pressures are in fact achieved by the concave stellated shells. Specifically, a geometrically perfect $5^{th}$-order stellated shell with $H = -0.2R$ can carry 46.5% larger external pressure than the perfect sphere.

The variation with $H$ and $n$ of the critical buckling modes for stellated shells is illustrated by Fig. 16. The $2^{nd}$-order stellated shells with shallow pyramids and $3^{rd}$-order stellated shells with concave and shallow convex pyramids exhibit

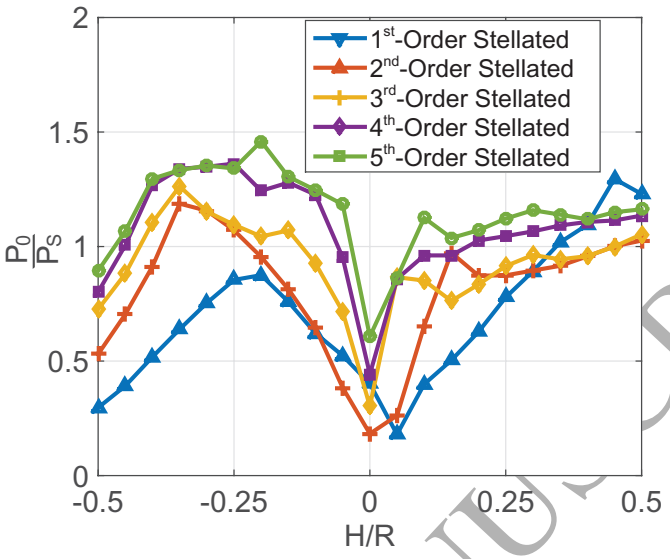


Figure 15: Variation of buckling pressure of geometrically perfect stellated shells ($P_0$) with pyramid height ($H$), normalized by buckling pressure of perfect sphere ($P_S$), for different order of subdivision.

5-fold rotational symmetry. The bucking modes of other shells are mostly rather localized.

The buckling pressure of geometrically perfect and imperfect $2^{nd}$- to $5^{th}$-order stellated shells, normalized by the buckling pressure of the perfect sphere, is plotted in Fig. 17. These results show that $2^{nd}$-order stellated shells are less sensitive to imperfections than higher-order stellated shells. The knockdown factors of $2^{nd}$-order stellated shells are higher than 0.87 for all values of $H$, except $0.15R < H < 0.35R$. Fig. 17 (a) also shows that the buckling pressure of imperfect shells in the ranges $-0.35R \leq H \leq -0.25R$ and $H \geq 0.45R$ are even higher than those of a perfect spherical shell. The $2^{nd}$-order stellated shell with $H = 0.5R$ can carry a buckling pressure of 1.03 times that of a perfect sphere with only 1% reduction due to imperfections. Geometrically imperfect $5^{th}$-order stellated shells with $H = -0.4R$ and $H = -0.25R$ can also carry a higher pressure than a perfect sphere. Their knockdown factors are 0.79 and 0.81, respectively.

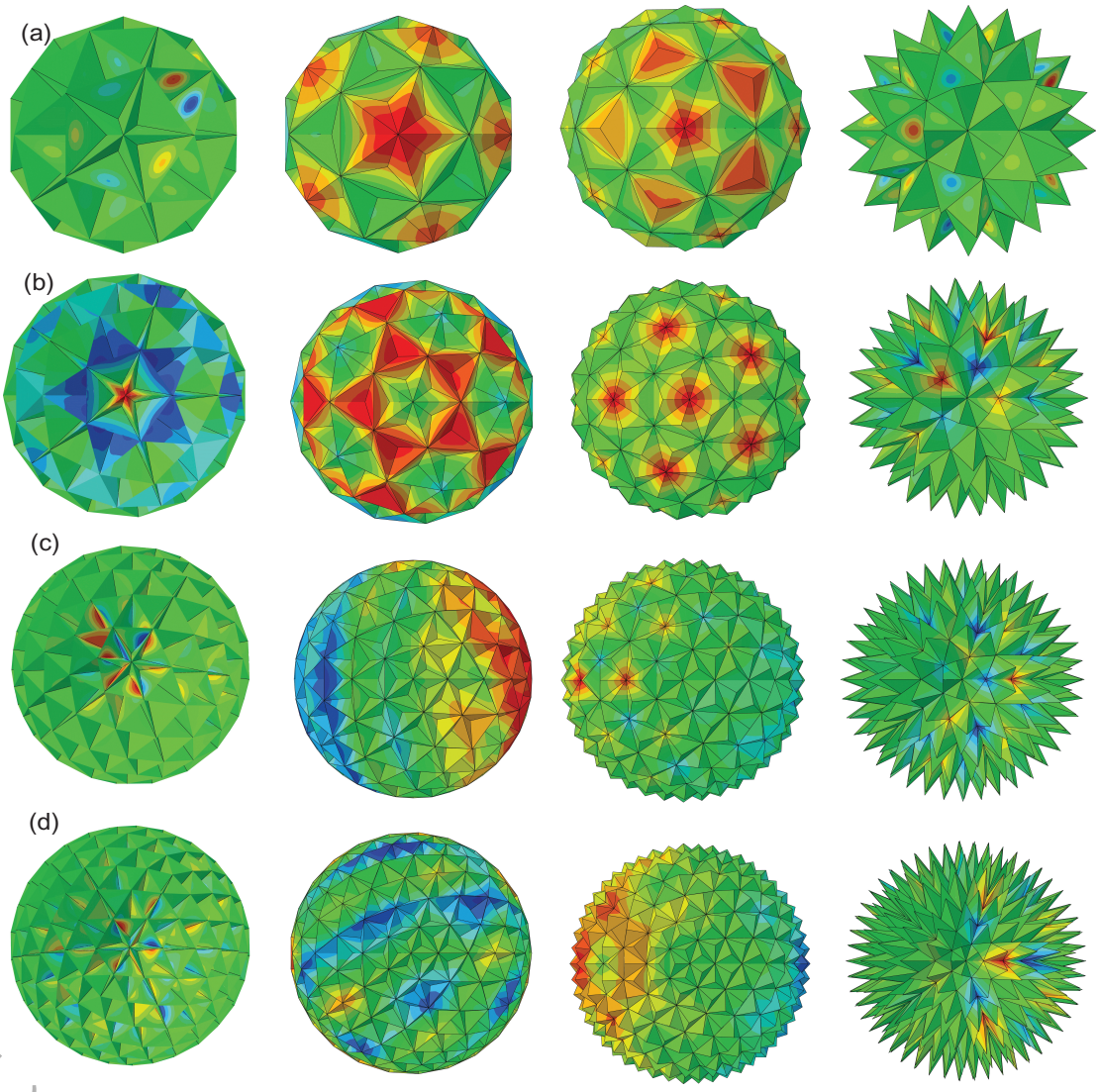


Figure 16: Variation of critical buckling mode from $n = 2$ (top) to $n = 5$ (bottom) and from $H = -0.5R$ (left), to $-0.1R$, $0.1R$ and to $H = 0.5R$ (right). The color contour represents radial deformation and outward deformation is shown in red.

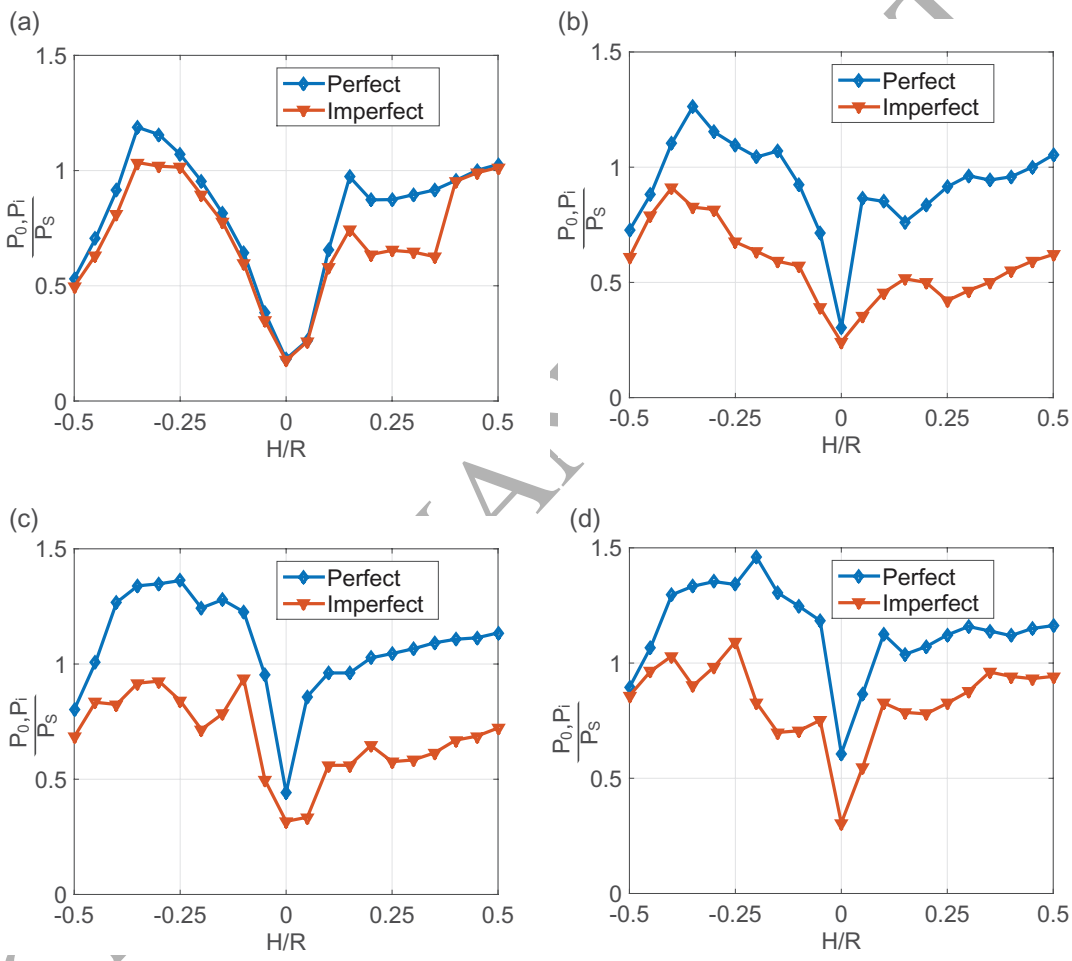


Figure 17: Variation of buckling pressure of geometrically perfect ($P_0$) and imperfect ($P_i$) $2^{nd}-$ to $5^{th}$-order stellated shells (Figs. a-d) with pyramid height ($H$), normalized by buckling pressure of perfect sphere ($P_S$), where $P_i = min(P_+, P_-)$.

In summary, the following results have been obtained for stellated shells. 1) The stellated geometry can significantly improve the load-carrying capability of near-spherical shells under external pressure and dramatically reduces their imperfection sensitivity. 2) Choosing optimal combinations of subdivision and pyramid height can achieve imperfection-insensitive designs with pressure carrying capability better than a geometrically perfect sphere.

For example, the $1^{st}$-order stellated shell with $H = 0.45R$ can carry an external pressure 28% higher than a perfect sphere with only 4.4% reduction due to imperfections. The $2^{nd}$-order stellated shell with $H = 0.5R$ is also an imperfection-insensitive design with higher buckling pressure than a perfect sphere.

### *4.3. Influence of Imperfection Amplitude*

Fig. 18 is a plot of the knockdown factors of stellated shells with various imperfection amplitudes, for fixed $R/t = 100$ and $H = 0.5R$.

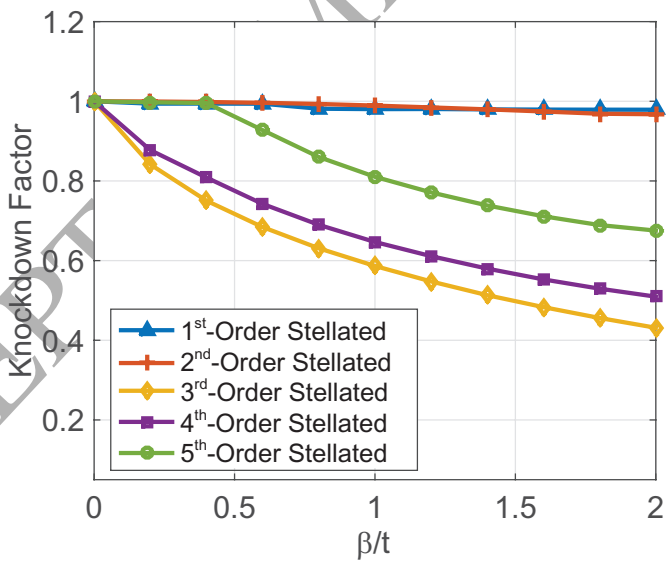


Figure 18: Knockdown factors of stellated shells with $H = 0.5R$ plotted against normalized imperfection amplitude.

The $1^{st}$- and $2^{nd}$-order stellated shells are insensitive to imperfections because their knockdown factors are reduced by only 4% even for the maximum imperfection amplitude of two shell thicknesses. However, significant reductions in knockdown factors of the $3^{rd}$- to $5^{th}$-order stellated shells are found when the imperfection amplitude increases, indicating that they are imperfection sensitive. A difference from the results for geodesic shells, shown in Fig. 11, is that the knockdown factors of stellated shells increase as the order of subdivision increases.

## 5. Mass Efficiency

Several potential designs for near-spherical shells that perform better than a sphere have been identified in the previous sections. Quantitative comparisons are now developed, using two mass efficiency metrics, the weight index and the load index, commonly used in comparisons of cylindrical shells (Peterson, 1967; Agarwal and Sobel, 1977; Nemeth and Mikulas, 2009).

The weight and load indices for cylindrical shells are defined as:

$$\text{Weight index}: \quad \frac{W}{AR} \tag{6}$$

$$\text{Load index}: \quad \frac{N_x}{R} \tag{7}$$

Here $W$, $A$, $R$ are the total weight, the surface area and radius of the cylinder, respectively. $N_x$ denotes the (axial) critical buckling stress resultant.

The same weight index can be used also for spherical shells, with the surface area is $A = 4\pi R^2$. Since the load index in Eq. 7 has the dimensions of pressure, it is replaced by the critical buckling pressure, denoted by $P_{cr}$.

For geometrically perfect spherical shells ($\gamma = 1$), the relation between weight and load indices can be found as follows. Begin by substituting $W = \rho A t$ into Eq. 6

$$\frac{W}{AR} = \frac{\rho t}{R} \tag{8}$$

Then, in Eq. 2 substitute $P_{cl} = P_{cr}$ and solve for $t$ to obtain:

$$t = R\sqrt{\frac{P_{cr}\sqrt{3(1-\nu^2)}}{2E}} \tag{9}$$

and substitute Eq. 9 into Eq. 8 to obtain:

$$\frac{W}{AR} = \rho\sqrt{\frac{\sqrt{3(1-\nu^2)}}{2E}}\sqrt{P_{cr}} \tag{10}$$

In logarithmic plots, Eq. 10 defines straight lines of slope 0.5, plotted as blue lines in Fig. 19. These lines set a design target for *mass-efficient imperfection-insensitive shells*. Designs closer to the right-bottom corner have higher efficiency because they can carry larger pressure with lower mass.

Fig. 19(a) is a plot of the load index vs. weight index for geometrically perfect and imperfect spherical shells (with $\gamma = 0.2$) and imperfect geodesic shells (with imperfection amplitude of one shell thickness). In this plot, imperfect spherical shells follow a straight line relationship, but shifted to the left because their buckling pressure is decreased by a factor of $\gamma = 0.2$.

The mass efficiencies of geodesic and stellated shells are compared with spherical shells through the load index ($P_{cr}$) and the weight index ($W/AR$). In the calculation of the weight indices for the near-spherical shells, $A$ and $R$ were set equal to the area and radius of the *circumscribed sphere*, respectively. $W$ and $P_{cr}$ were respectively the mass and critical buckling pressure for each shell. Note that the values of $P_{cr}$ shown in these charts correspond to geometrically imperfect geometries. Geometrically perfect near-spherical shells were not included in these comparisons.

Fig. 19(a) shows that the mass efficiency of the $1^{st}$-order geodesic shell (icosahedron) is higher than any other geodesic shell. The $2^{nd}$- and $3^{rd}$-order geodesic shells have similar efficiency, close to imperfect spherical shells. The $4^{th}$- and $5^{th}$-order geodesic shells have similar mass efficiency, higher than the $2^{nd}$- and $3^{rd}$-order shells. The dash-line in the figure defines a geometrically imperfect sphere that has the same mass efficiency as the best $1^{st}$-order geodesic shell. *The knockdown factor for this best in category design is 0.75.* This result indicates that the efficiency of the $1^{st}$-order geodesic shell is only 25% lower than a geometrically perfect sphere.

Fig. 19(b) compares the mass efficiency of $1^{st}$-order stellated shells with different pyramid heights to $1^{st}$-order geodesic shells and smooth spheres. The

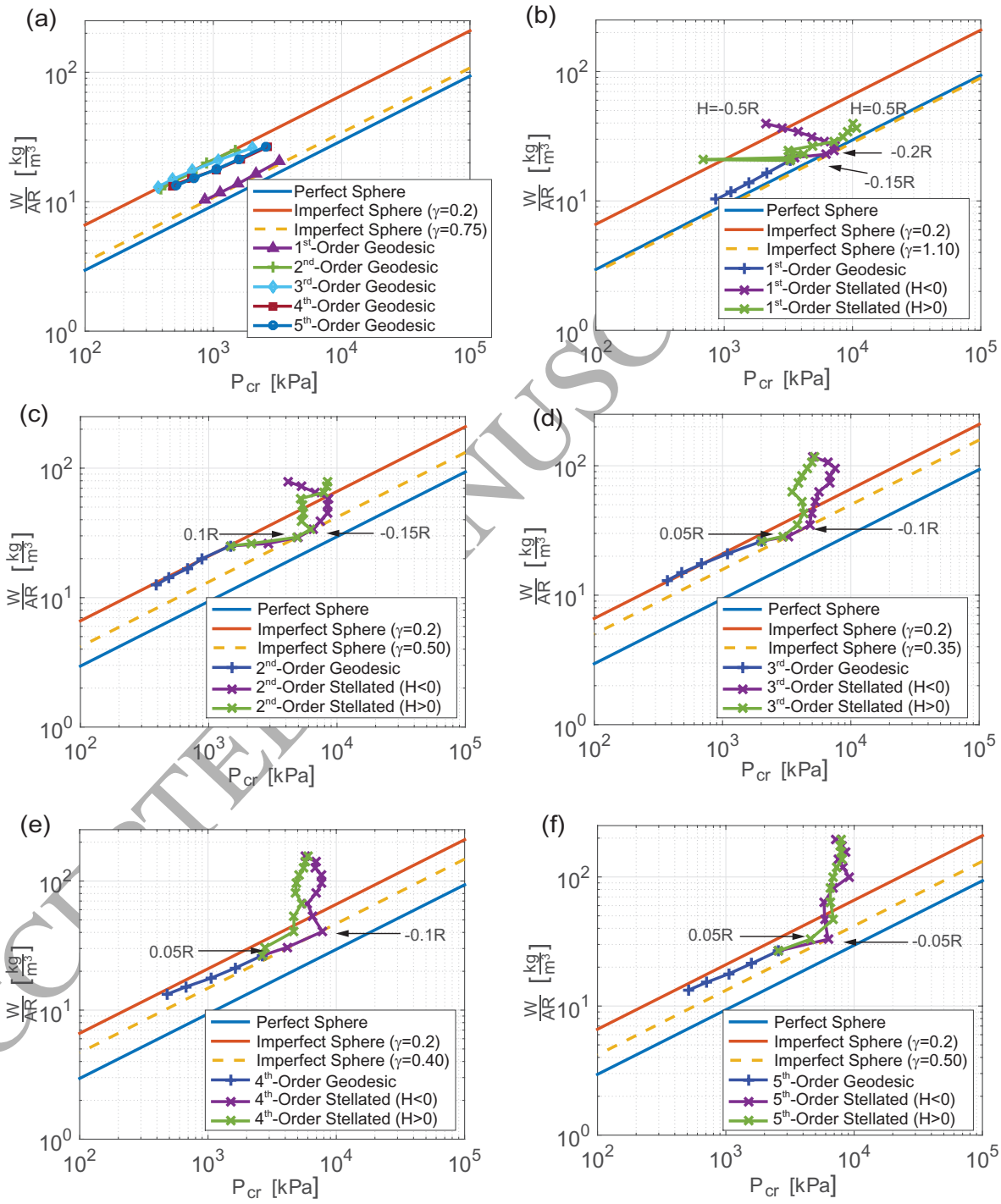


Figure 19: Mass efficiency of geodesic shells (a) and stellated shells (b-f). The dash lines define geometrically imperfect spherical shells with the same mass efficiency as the best near-spherical shell in the category.

stellated shell with $H = -0.5R$ has the lowest mass efficiency. Then, as $H$ increases, the efficiency also increases until $H = -0.2R$, and then decreases until $H = 0.05R$. These results indicate that many $1^{st}$-order stellated shells have higher mass efficiency than $1^{st}$-order geodesic shells, which were the best performing design in Fig. 19(a). It particular, the $1^{st}$-order stellated shells with $H = -0.2R$ and $H = -0.15R$ are the best performing, and the dash line that marks *the best in category design corresponds to a knockdown factor of 1.10*. These designs have higher mass efficiency than perfect spheres.

Figs. 19(c-f) show plots of the mass efficiency of $2^{nd}$- to $5^{th}$-order stellated shells. Each plot includes also the corresponding geodesic shells, the perfect sphere, and imperfect sphere with a knockdown factor of 0.2. The results presented in these plots indicate that shallow convex or concave stellations can achieve higher mass efficiency than imperfect spherical shells and geodesic shells and that deeper stellations lead to lower mass efficiency. In addition, none of the stellated shells reaches the mass efficiency of the perfect sphere. Moreover, the number of stellated geodesic shells with higher mass efficiency than the corresponding geodesic shell decreases as the order of stellated geodesic shell increases, showing that the effects of stellation on improving mass efficiency are weakened for higher-order stellated shells.

## 6. Volume Efficiency

There are many applications of spherical shells that require not only ability to carry high pressure with low weight, but also high enclosed volume. Typical examples are spherical domes in architecture, deep-sea vehicles, and micro-scale capsules for drug delivery. These applications can be addressed by considering the volume efficiency of near-spherical shells.

The volume index, which quantifies the volume efficiency of a particular design, is defined as:

$$\text{Volume index}: \quad \frac{V}{W} \tag{11}$$

where $V$ is the volume enclosed by the shell and $W$ denotes its mass. A larger

value of the volume index corresponds to designs that provide higher internal volume with smaller amount of material. The critical buckling pressure, $P_{cr}$, is still used as the load index.

For perfect spherical shells, the relation between volume index and load index can be found as follows. Begin by substituting $V = \frac{4\pi R^3}{3}$ and $W = 4\pi R^2 t\rho$ into Eq. 11, to obtain

$$\frac{V}{W} = \frac{1}{3\rho}\frac{R}{t} \tag{12}$$

Then, substitute Eq. 9 into Eq. 12 to obtain:

$$\frac{V}{W} = \frac{1}{3\rho}\sqrt{\frac{2E}{\sqrt{3(1-\nu^2)}}}{P_{cr}}^{-\frac{1}{2}} \tag{13}$$

Fig. 20 shows a series of logarithmic plots of load index vs. volume index for all shells studied in this paper. In these plots, shells with larger values of load and volume indices have higher volume efficiency, and therefore, the shells located closer to the top-right corner of these volume efficiency charts are more efficient.

Fig. 20(a) investigates the volume efficiency of geodesic shells, and includes also perfect spheres and imperfect spheres with a knockdown factor $\gamma = 0.2$. This chart shows that the geodesic shells have comparable volume efficiency to the imperfect sphere.

Fig. 20(b) compares the volume efficiencies of $1^{st}$-order stellated shells with different heights to the corresponding geodesic shells, and to the sphere. Predictably, convex stellated shells ($H > 0$) can achieve the highest volume efficiency, whereas concave stellated shells ($H < 0$) have lower volume efficiency. The stellated shell with $H = 0.45R$ has the highest volume efficiency, and is equivalent to a spherical shell with $\gamma = 0.65$ as shown by the dash line.

Figs. 20(c-f) present volume efficiency comparisons for $2^{nd}$- to $5^{th}$-order stellated shells. These results show that in the case of higher-order subdivision, stellation improves volume efficiency for shallow convex and concave pyramids, whereas for deep pyramids it reduces volume efficiency. The most efficient $2^{nd}$- to $5^{th}$-order stellated shells are equivalent to spheres respectively with

$\gamma = 0.5,\ 0.31,\ 0.32,\ 0.45$. The most efficient among $2^{nd}$- and $3^{rd}$-order stellated shells have convex pyramids ($H = 0.15R$ and $H = 0.05R$, respectively). However, the $4^{th}$- and $5^{th}$-order stellated shells with concave pyramids ($H = -0.05R$ and $H = -0.05R$, respectively) are actually the most efficient, although they are less efficient than the previously identified (Fig. 20(b) ) $1^{st}$-order stellated shell.

## 7. Conclusion

The buckling and imperfection sensitivity of two families of near-spherical shells, geodesic shells and stellated shells with different orders of subdivision, have been studied and compared to spherical shells. Their mass and volume efficiencies have also been studied.

For geometrically perfect geodesic shells, it has been found that —as the order of subdivision increases— the critical buckling pressure initially decreases and then increases, and is always lower than a geometrically perfect sphere. For any chosen order of subdivision, the critical buckling pressure decreases with a power law with respect to the radius-to-thickness ratio. When geometric imperfections are accounted for, the knockdown factor decreases when the order of subdivision is increased. Considering these effects together, $1^{st}$-order geodesic shells are the best performers, and can carry external pressure significantly higher than a spherical shell. The buckling modes of geodesic shells transition from mirror symmetry to 5-fold rotational symmetry as the order of subdivision is increased.

Stellated shells are generally insensitive to imperfections, and the height of the pyramids can be used as an additional design parameter to maximize the buckling pressure, although its variation with $H$ is rather complex. Shells with $1^{st}$-order subdivision and pyramid heights of $-0.3R$ (concave shell) and $+0.45R$ (convex shell) have the highest critical buckling pressures. For $H \geq 0.35R$ the buckling pressure is always greater than for a perfect sphere, and for $H = 0.45R$ (highest buckling pressure) it is 28% higher. $2^{nd}$-order stellated shells are also

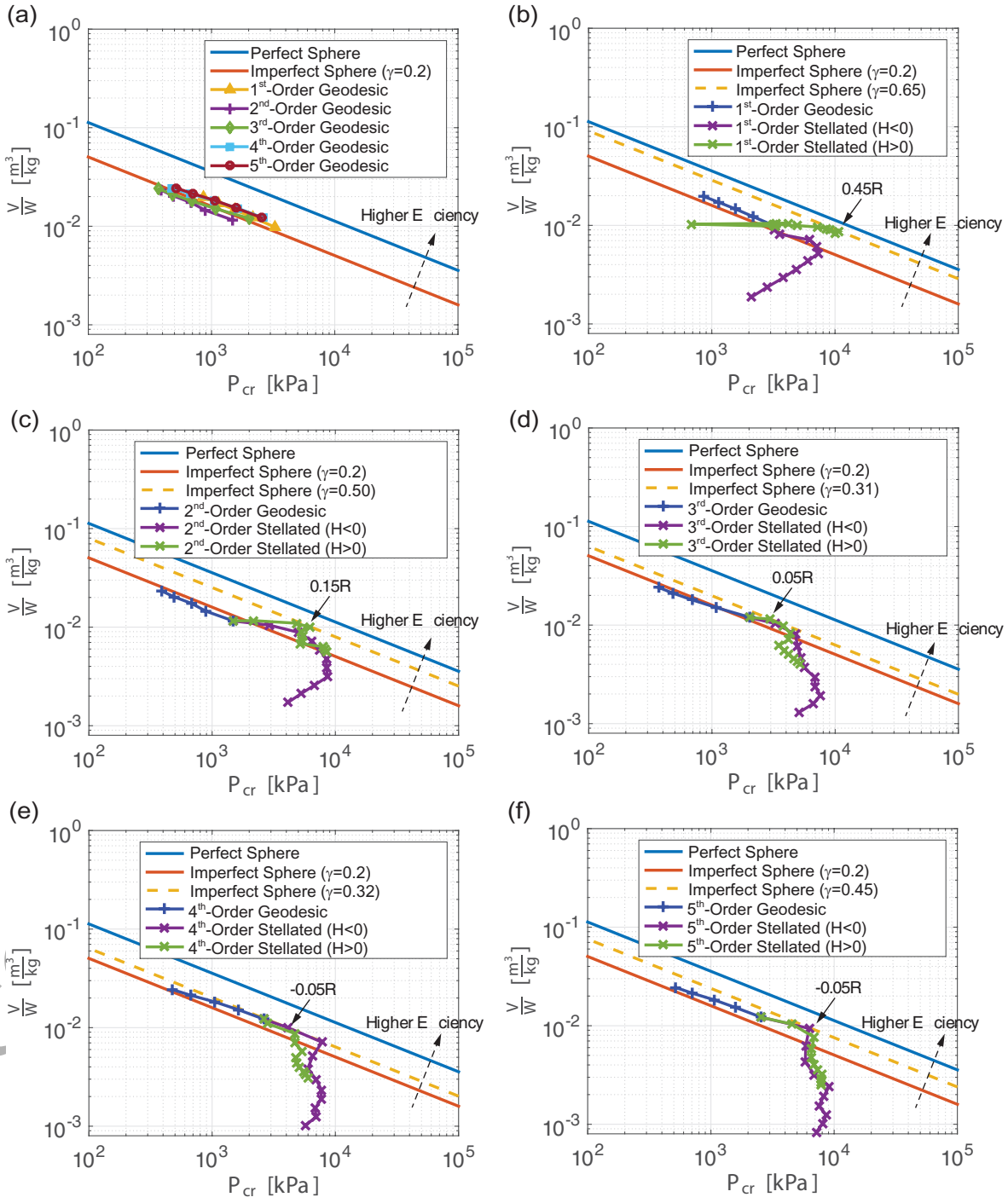


Figure 20: Volume efficiency charts for (a) geodesic shells and (b-f) $1^{st}$- to $5^{th}$-order stellated shells. The dash arrows indicate regions with higher volume efficiency. The value of $H$ corresponding to the most efficient near-spherical shell is marked in each figure. The dash lines define geometrically imperfect spherical shells with the same volume efficiency as the best near-spherical shell in the category. The data for all near spherical shells assumes as imperfection amplitude of one shell thickness.

insensitive to imperfections (the knockdown factor is 0.99), however higher-order shells are more sensitive to imperfections. The bottom line is that stellated shells can carry higher external pressures than geodesic shells.

The mass efficiency of geodesic and stellated shells was studied by plotting maps of weight index vs. critical buckling pressure. It was found that the $1^{st}$-order geodesic shell (icosahedron) has the highest mass efficiency among all geodesic shells. Geodesic shells are at least as efficient than geometrically imperfect spheres, but they are less efficient than a perfect sphere. The stellated geometry significantly improves the mass efficiency and, in particular, $1^{st}$-order stellated shells with concave pyramids ($H = -0.2R$ and $H = -0.15R$) are more efficient than even the perfect sphere. Stellated shells with shallow pyramids are more efficient than the corresponding geodesic shells, but less efficient than the perfect sphere. It was also found that the effects of improving mass efficiency by stellation are reduced when the order of geodesic shells is increased.

The volume efficiency of geodesic and stellated shells was also studied by plotting maps of the volume index vs. the critical buckling pressure. Geodesic shells are comparable to imperfect spherical shells with a knockdown factor of 0.2. $1^{st}$-order convex stellated shells perform much better, being comparable to imperfect spherical shells with a knockdown factor of 0.65. In terms of volume efficiency, this is the best result from the present study.

In concluding, three last points should be noted. First, in the present study the shape of the imperfections was based on the critical buckling mode and the material behavior assumed linearly elastic. In future, it would be worth studying the effects of alternative shapes of imperfections and also of material non-linearity. Second, while the present study has focused exclusively on numerical investigations, experimental verification of key results is a necessary next step. Third, the results presented in this paper suggest that further exploration of other kinds of near-spherical shells, including shells with reinforcing frames/stiffeners, composite shells with tailored material properties, and variants of other platonic polyhedra should be considered.

**References**

Adorno-Rodriguez, R., Palazotto, A.N., 2015. Nonlinear structural analysis of an icosahedron under an internal vacuum. J. Aircraft, 52, 878-883.

Agarwal, B.L., Sobel, L.H., 1977. Weight optimized stiffened, unstiffened, and sandwich cylindrical shells. J. Aircraft, 14, 1000-1008.

Carlson, R.L., Sendelbeck, R.L., Hoff, N.J., 1967. Experimental studies of the buckling of complete spherical shells. Exp. Mech., 7, 281-288.

Datta, S.S., Kim, S.H., Paulose, J., Abbaspourrad, A., Nelson, D.R. Weitz, D.A., 2012. Delayed buckling and guided folding of inhomogeneous capsules. Phys. Rev. Lett., 109, 134302.

Fuller, R.B., 1965, Geodesic structures. US Patent 3197927 A.

Hoff, N.J., Soong, T.C., 1963. Lower bounds for the buckling pressure of spherical shells. NASA Technical Report, NASA-CR-50600, SUDAER-133.

Homewood, R.H., Brine, A.C., Johnson, A.E., Jr., 1961. Experimental investigation of the buckling instability of monocoque shells. Exp. Mech., 1, 8896.

Hutchinson, J.W., 1967. Imperfection sensitivity of externally pressurized spherical shells. J. Appl. Mech., 34, 49 - 55.

Hutchinson, J.W., 2016. Buckling of spherical shells revisited. Proc. R. Soc. A, 472, 20160577.

Jimenez, F.L., Marthelot, J., Lee, A., Hutchinson, J.W., Reis, P.M., 2016. Knockdown factor for the buckling of spherical shells containing large-amplitude geometric defects. J. Appl. Mech., 84, 034501-1 -4.

Jose, J., Kamp, M., van Blaaderen, A., Imhof, A., 2014. Unloading and reloading colloidal microcapsules with apolar solutions by controlled and reversible buckling. Langmuir, 30, 2385-2393.

Kaplan, A., Fung, Y.C., 1954. A nonlinear theory of bending and buckling of thin elastic shallow spherical shells, NASA Technical Note 3212.

Kitrick, C.J., 1983. Nonlinear analysis of normal and inverted geodesic domes under the action of concentrated loads. Master thesis, University of Cincinnati.

Kim, S.H., Park, J.G., Choi, T.M., Manoharan, V.N., Weitz, D.A., 2014. Osmotic-pressure-controlled concentration of colloidal particles in thin-shelled capsules. Nat. Commun., 5, 3068.

Klug, W.S., Bruinsma, R.F., Michel, J.P., Knobler, C.M., Ivanovska, I.L., Schmidt, C.F., Wuite, G.J., 2006. Failure of viral shells. Phys. Rev. Lett., 97, 228101.

Koga, T., Hoff, N.J., 1969. The axisymmetric buckling of initially imperfect complete spherical shells. Int. J. Solids Struct., 5, 679 - 697.

Koiter WT. 1945. On the stability of elastic equilibrium. Dissertation, Delft, The Netherlands.

Krenzke, M.A., 1962. Tests of machined deep spherical shells under external hydrostatic pressure. Technical Report DTMB-1601, The David Taylor Model Basin, Washington, D.C.

Krenzke, M.A., Kiernan, T.J., 1963. Tests of stiffened and unstiffened machined spherical shells under external hydrostatic pressure. Technical Report DTMB-1741, The David Taylor Model Basin, Washington, D.C.

Lana-Terzi, F.,1670. Prodromo. Edited by Andrea Battistini, Milan, Longanesi Publishers, 1978.

Lee, A., Brun, P.T., Marthelot, J., Balestra, G., Gallaire, F., Reis, P.M., 2016. Fabrication of slender elastic shells by the coating of curved surfaces. Nat. Commun., 7, 11155

Lee, A., Jimenez, F.L., Marthelot, J., Hutchinson, J.W., Reis, P.M., 2016. The geometric role of precisely engineered imperfections on the critical buckling load of spherical elastic shells. J. Appl. Mech., 83, 111005.

Lidmar, J., Mirny, L. and Nelson, D.R., 2003. Virus shapes and buckling transitions in spherical shells. Phys. Rev. E, 68, 051910.

Mannige, R.V., Brooks, C.L., 2009. Geometric considerations in virus capsid size specificity, auxiliary requirements, and buckling. Proc. Natl. Acad. Sci., 106, 8531-8536.

May, E.R., Brooks III, C.L., 2012. On the morphology of viral capsids: elastic properties and buckling transitions. J. Phys. Chem. B, 116, 8604-8609.

Metlen, T.T., 2012. Design of a lighter than air vehicle that achieves positive buoyancy in air using a vacuum. Master's thesis, Air Force Institute of Technology, AFIT-ENY-13-J-02.

Nemeth, M.P., Starnes, J.H., 1998. The NASA monographs on shell stability design recommendations: a review and suggested improvements. NASA Technical report, TP-1998-206290.

Nemeth, M., Mikulas, M.M., 2009. Simple formulas and results for buckling-resistance and stiffness design of compression-loaded laminated-composite cylinders. NASA Technical report, TP-2009-215778.

Ning, X., Pellegrino, S., 2013. Imperfection-Insensitive Axially Loaded Cylindrical Shells. 54th AIAA/ASME/ASCE/AHS/ASC Structures, Structural Dynamics and Materials Conference. Boston, MA, AIAA-2013-1768.

Ning, X., Pellegrino, S., 2015. Imperfection insensitive axially loaded thin cylindrical shells. Int. J. Solids Struct., 62, 39-51.

Ning, X., 2015. Imperfection insensitive thin shells. Doctoral dissertation, California Institute of Technology.

Ning, X., Pellegrino, S., 2016. Bloch wave buckling analysis of axially loaded periodic cylindrical shells. Comput. Struct., 177, 114-125.

Ning, X., Pellegrino, S., 2017. Experiments on imperfection insensitive axially loaded cylindrical shells. Int. J. Solids Struct., 115, 73-86.

Peterson, J.P., 1967. Structural efficiency of ring-stiffened corrugated cylinders in axial compression. NASA Technical note, TN D-1073.

Ru, C.Q., 2009. Buckling of empty spherical viruses under external pressure. J. Appl. Phys., 105, 124701.

Seaman, L., 1962. The nature of buckling in thin spherical shells. Doctoral dissertation, Massachusetts Institute of Technology, Cambridge, MA.

Siber, A., Podgornik, R., 2009. Stability of elastic icosadeltahedral shells under uniform external pressure: application to viruses under osmotic pressure. Phys. Rev. E, 79, 011919.

Singer, J., Arbocz, J., Weller, T., 2002. Buckling experiments: experimental methods in buckling of thin-walled structures: Vol. 2. Wiley, New York, NY.

Snyder, J.W., Palazotto, A.N., 2017. Design and Modal Analysis of a Unique Structure under an Internal Vacuum", 58th AIAA/ASCE/AHS/ASC Structures, Structural Dynamics, and Materials Conference, AIAA SciTech Forum, (AIAA 2017-1596) https://doi.org/10.2514/6.2017-1596

Tarnai, T., 1989. Buckling patterns of shells and spherical honeycomb structures. Computers & Mathematics with Applications, 17(4-6), 639-652.

Tarnai, T., 1996. Geodesic domes: natural and man-made. Int. J. Space Structures, 11, 13-25.

Thompson, J.M.T., 1960. Making of thin metal shells for model stress analysis. J. Mechanical Engineering Science, 2, 105-108.

Thompson, J.M.T., and Hutchinson, J.W., 2017. Nonlinear buckling interaction for spherical shells subject to pressure and probing forces. Submitted.

Van Loon, B., 1994. Geodesic domes. Parkwest Publications, 1994.

Vliegenthart, G.A., Gompper, G., 2011. Compression, crumpling and collapse of spherical shells and capsules. New J. Phys., 13, 045020.

Ventsel, E., Krauthammer, T., 2001. Thin plates and shells: theory: analysis, and applications. CRC Press, New York, NY.

Von Kármán, T., Tsien, H.S., 1939. The buckling of spherical shells by external pressure. Journal of the Aeronautical Sciences, 7, 43-50.

Zoelly, R., 1915. Über ein Knickungsproblem an der Kugelschale. Doctoral Dissertation, ETH Zürich.